Intertidal Regions Regulate Seasonal Coastal Carbonate System Dynamics in the East Frisian Wadden Sea

Julia Meyer^{1, 3}, Yoana G. Voynova¹, Bryce Van Dam¹, Lara Luitjens², Dagmar Daehne², Helmuth Thomas^{1, 3}

- ¹ Institute of Carbon Cycles, Helmholtz-Zentrum Hereon, Geesthacht, 21502, Germany
 - ² Lower Saxony department of water management, coastal protection and nature protection (NLWKN), Norden, 26506, Germany
 - ³ Institute for Chemistry and Biology of the Marine Environment (ICBM), Carl von Ossietzky Universität Oldenburg, 26111 Oldenburg, Germany
- 10 Correspondence to: Julia Meyer (julia.meyer@hereon.de)

Abstract. Seasonal and regional changes in carbon dynamics in the Wadden Sea, the world's largest intertidal sand and mud flats system, were analysed to quantify the influence of biogeochemical processes on the carbonate system at the land-sea interface. With a focus on the East Frisian Wadden Sea (EFWS), we successfully used the difference between total alkalinity (TA) and dissolved inorganic carbon (DIC) ([TA-DIC]), as well as the calculated parameters ΔTA_{excess}, ΔDIC_{excess} and ΔTA_P to identify how ongoing biogeochemical processes regulate the carbonate system dynamics.

In spring, a phytoplankton bloom with high biological activity, indicated by (a) supersaturated oxygen (up to 180 in % saturation), (b) elevated chlorophyll a (up to 151.7 μ g L⁻¹) and (c) low pCO₂ (as low as 141.3 μ atm), resulted in decrease in nitrate (NO₃⁻, 19.29 \pm 18.11 μ mol kg⁻¹) and DIC (159.4 \pm 125.4 μ mol kg⁻¹), and a slight increase in TA (9.1 \pm 29.2 μ mol kg⁻¹). The regression analysis of the differences between March and May 2022 in NO₃⁻ concentrations (Δ NO₃⁻) against the differences in DIC (Δ DIC) yielded a slope of 6.90, matching the Redfield C:N ratio, and suggesting that uptake of nitrate by primary producers increased total alkalinity during the spring bloom.

In summer, we assume that organic matter remineralization, along with $CaCO_3$ dissolution in sediments, enhances TA production in the coastal and nearshore regions of the Western EFWS (up to 2400 μ mol kg⁻¹). In the Eastern EFWS, enhanced $CaCO_3$ formation may consume TA ([TA-DIC] < 200 μ mol kg⁻¹), but the region still acts as a net source of TA, likely due to sedimentary processes such as organic matter decomposition, which follow the time of increased biological activity during the spring bloom. The increase of TA enhances the coastal ocean's ability to absorb and store CO_2 through buffering and suggests that the EFWS can be a source of TA to the coastal regions during the warm productive seasons. This study highlights the complex relationships between these factors, emphasizing the need for a comprehensive understanding of regional and seasonal variations to better assess the role of coastal systems in carbon cycling, storage and climate regulation.

30 1 Introduction

Coastal oceans are biogeochemically active regions, which play a significant role in biogeochemical cycles, despite covering less than 10 % of the oceanic realm (Gattuso et al., 1998). Coastal regions are directly affected by terrestrial organic matter and nutrients through river run-off, groundwater discharge, atmospheric deposition, and exchange of large amounts of matter and energy with the open ocean (Borges et al., 2006; Gattuso et al., 1998). Overall, coastal oceans also support approximately 14 - 23 % of the ocean carbon dioxide uptake, 10 - 30 % of the primary production, 80 % of organic matter burial, 90 % of sedimentary mineralization and 75 - 90 % of the oceanic sink of suspended river loads (Bauer et al., 2013; Gattuso et al., 1998). Since the start of the industrial era, the levels of CO₂ in the atmosphere have increased from ~280 ppm to over ~419 ppm due to human activities (Friedlingstein et al., 2023). About 30 % of anthropogenic CO₂ emissions since the industrial period have been absorbed by the ocean (Friedlingstein et al., 2023). The uptake increases the concentration of protons [H⁺] and decreases the carbonate ion concentration [CO₃²⁻], leading to lower pH and a reduced saturation state of calcium carbonate, a process known as ocean acidification (Orr et al., 2005). Depending on the different model scenarios, it is predicted that surface pH in the ocean might decline by about 0.3 - 0.4 pH units by 2100, corresponding to a decrease of about 40 - 50 % of carbonate ions in the seawater (Feely et al., 2009; Orr et al., 2005). The future capacity of the ocean to take up CO₂, can affect the precipitation and dissolution of the carbonate minerals, as well as the survival of marine organisms (Duan et al., 2023; Kroeker et al., 2013; Liang et al., 2023; Ricour et al., 2023). Whereas oceans are a significant sink for anthropogenic CO₂ it is not well known how this uptake will further change under the continual increase of anthropogenic CO₂ in the atmosphere (Lorkowski et al., 2012; Sabine et al., 2004; Thomas et al., 2007). However, rising atmospheric CO₂ will influence carbon stocks and fluxes in the pelagic, benthic and coastal zone, particularly in shelf seas, which are annually mixed and ventilated (Legge et al., 2020). Total alkalinity (TA) represents the buffering capacity of the ocean and is controlled by many factors including erosion/weathering pathways on land (Lehmann et al., 2023) and respiration of organic matter (OM) along anaerobic metabolic pathways, mostly generated in shallow marine and shelf sediments (Dickson, 1981). These processes are directly influenced by terrestrial and anthropogenic nutrient inputs (Van Beusekom and De Jonge, 2002; Burt et al., 2016; Thomas et al., 2009), as well as increased sedimentation of reactive organic matter (OM) (Al-Raei et al., 2009; Böttcher et al., 1998). Coastal seas and shelf seas, like the North Sea often have relatively high rates of primary production in spring, leading to drawdown in DIC, pCO₂ and a consequent pH increase (Macovei et al., 2021; Thomas et al., 2005). In addition, nutrient loads from land contribute to enhanced primary production, and increased carbon remineralization (Prowe et al., 2009; Thomas et al., 2009), and subsequent changes in the carbonate system. Previous studies suggested that the Wadden Sea, a large network of intertidal sand and mudflats bordering the North Sea along the Dutch, German and Danish coasts (Staneva et al., 2009), plays a significant role in modulating local carbonate system dynamics (Thomas et al., 2009; Voynova et al., 2019). The seasonal TA production in the southern North Sea, exhibited a regional TA variability, which was attributed to the influence of the Wadden Sea (Voynova et al., 2019), and to benthic TA production (Brenner et al., 2016). The observed seasonal changes of TA can affect the coastal ocean capacity to absorb carbon from the atmosphere (Burt et al., 2016; Gruber et al., 2019; Li et al., 2024; Schwichtenberg et al., 2020).

This study offers a detailed analysis of seasonal and inter-annual carbonate system dynamics in the EFWS, a key region within the world's largest intertidal sand and mudflat system (UNESCO World Heritage Centre, n.d.). As an essential component of coastal carbon cycling, and a land-sea junction, this area requires a deeper understanding of the processes influencing TA and DIC. The research focuses on seasonal and regional variations, and particularly on the drivers of TA production in spring-summer. By examining changes in TA, DIC, and other biogeochemical parameters, this study identifies key mechanisms affecting carbonate chemistry, including calcium carbonate (CaCO₃) dissolution and formation, photosynthesis and respiration. Our findings highlight the complex interactions among these factors, emphasizing the need for a comprehensive understanding of regional and seasonal variations to better assess the role of coastal systems in carbon cycling, storage, and climate regulation. Moreover, observed TA and DIC distributions provide valuable insights into potential carbon and TA sources within this dynamic environment.

2 Material and Methods

5 2.1 Study Side

85

The German Bight region is bordered by Germany, Denmark and the Netherlands, situated in the southeastern corner of the North Sea (Fig. 1a). The East Frisian Wadden Sea (EFWS) is one of the shallowest regions of the German Bight, characterized by a series of barrier islands (Fig. 1b), each 5 - 17 km long and 2 - 3 km wide (Staneva et al. 2009). The system is an intertidal region, influenced by semidiurnal tides with a tidal range from approximately 2.2 - 2.8 m (Grunwald et al. 2009; Staneva et al. 2009) and up to ~ 3.5 m in the Elbe River mouth (Staneva et al. 2009).

We separated the study area in two regions (Western WS & Eastern WS; Fig. 1b) due to the differences in the tidal dynamics and hydrodynamic properties (Herrling and Winter, 2015), which drive the area's carbon dynamics, sediment transport, and overall ecological functioning. The tidal range increases from 2.4 m at Borkum to 3.0 m at Wangerooge, with the Eastern region experiencing stronger tidal influences (Herrling and Winter, 2015). In the Langeoog basin, wind effects cause the largest relative increase in residual discharge, while Norderney experiences the largest absolute increase in water flux. Westerly winds influence residual circulation and sediment transport differently in each region. The flow dynamics between the basins of Baltrum and Langeoog are interconnected, whereas the flow regime between Borkum and Norderney is more independent from the dominant circulation patterns and inter-basin exchange (Herrling and Winter, 2015).

Seasonal cruises were completed in the Wadden Sea (WS) and North Sea around the East Frisian Islands (and the Ems River estuary) with the research vessel (RV) *Burchana* (Lower Saxony department of water management, coastal protection, and nature protection (NLWKN; Fig. 1b). The July 2021 and October 2021 cruises focused exclusively on the intertidal mudflats of the EFWS. The RV *Burchana*, with a draft of 1.3 meters, allowed sea water sampling even during low tide, providing the

opportunity to collect samples at various tidal stages. Sampling took place during daylight hours, typically starting in the morning at low tide and continuing throughout the day, with no nighttime samples collected. Both shallow intertidal areas (accessible due to the vessel's low draft) and deeper subtidal channels were sampled to ensure comprehensive spatial coverage. Later cruises extended into the Ems River Estuary, from the island of Borkum (Bork, Fig. 1b) to Weener (53°09'55.4"N 7°20'39.9"E), a town located upstream the Ems River. These additional data from the Ems River will be presented in a subsequent paper.

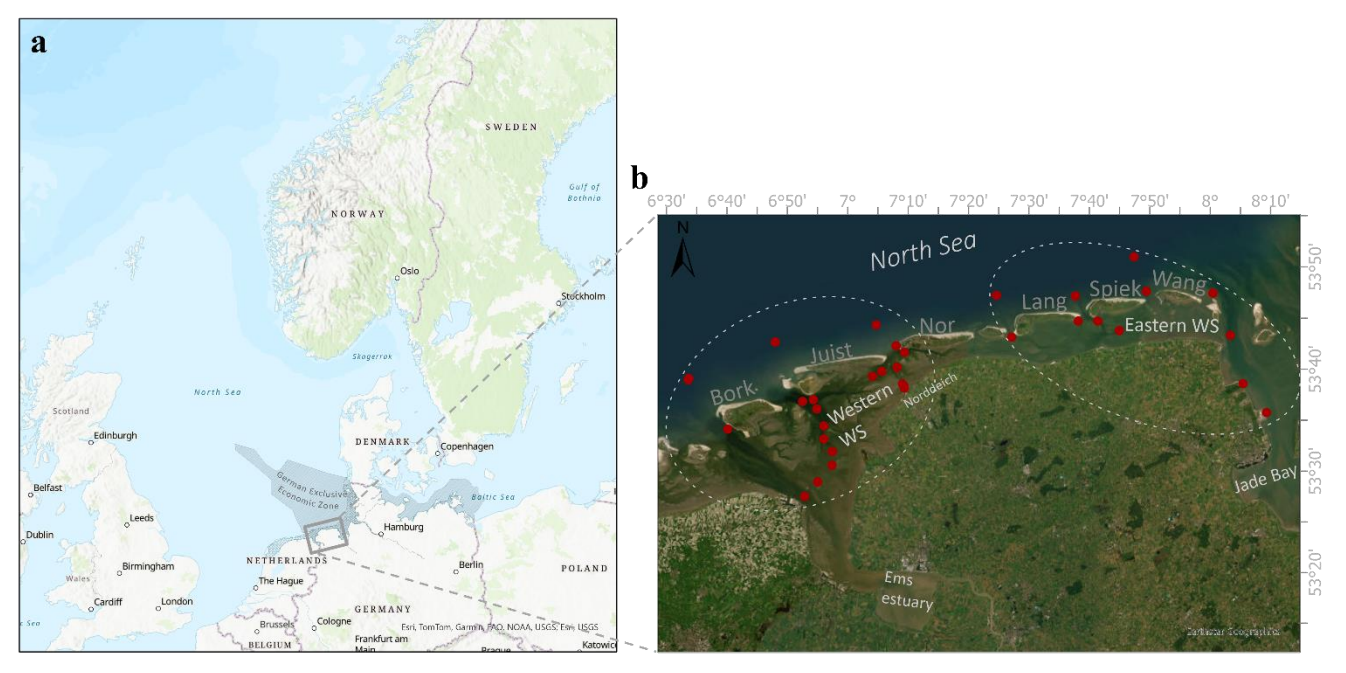


Figure 1: Study area, (a) The German Wadden Sea (=WS), (shown in grey) with the German Exclusive Economic Zone (hatched region) and the EFWS region (grey box). (b) Zoom into the EFWS, showing the sampling stations (red dots) in the different regions (Western WS and Eastern WS) considered in this study. The different Islands are labelled with the first few letters of their names (Bork= Borkum, Juist, Nor= Norderney, Lang= Langeoog, Spiek= Spiekeroog, Wang= Wangeoog). The map in this Figure was generated using ArcGIS. Data sources: (a) Esri, TomTom, Garmin, FAO, NOAA, USGS; (b) Earthstar Geographics. © 2024 Julia Meyer.

2.2 FerryBox measurements

110

A FerryBox system (4H-JENA engineering GmbH, Jena, Germany) was operated during all cruises on board the *RV Burchana* (NLWKN), measuring the following parameters every minute: temperature (SBE38, Sea-Bird Scientific), salinity (SBE45, Sea-Bird Scientific), dissolved oxygen (DO) (Optode 4835, Aanderaa, Bergen, Norway), chlorophyll fluorescence to estimate chlorophyll a concentrations (AlgaeOnlineAnalyser, bbe moldaenke), pH (electrode, Xylem; measured on total scale) and turbidity (Solitax inline SC, Hach Lange). The pH electrode was calibrated using standard DuraCal buffer solutions at pH 7 and pH 10 (Hamilton Company, USA). The partial pressure of CO₂ (*p*CO₂) was measured using a sensor (HydroC CO₂-FT, 4H-JENA engineering) attached to the flow-through system of the FerryBox. The data were corrected using the data processing

manual of 4H - Jena Engineering GmbH (4H Jena, 2021). Regions near the ports were excluded in all datasets, to remove any influence from the port, or from the cleaning cycles.

2.3 Discrete samples

120

130

135

Samples for Winkler titration (dissolved oxygen), nutrients, salinity and turbidity were collected from each cruise to crosscheck the measurements of the FerryBox. Therefore, dissolved oxygen (DO) samples were collected on the last day of each cruise by filling Biological Oxygen Demand (BOD) bottles from the FerryBox outflow. Three replicates collected underway were treated according to the standard Winkler method and measured within 24 hours in the lab using a Metrohm 870 KF Titrino Plus. The Winkler titrations were used to correct the FerryBox dissolved oxygen measurements from the seasonal cruises. A single regression equation for the Winkler titrations and the FerryBox data was used to apply a dissolved oxygen correction of the entire data set (y= 1.17x - 31.89, R²= 0.98, n= 46). In addition, the apparent oxygen utilization (AOU) was calculated using the corrected oxygen measurements, as according to:

125
$$AOU = O_2' - O_2$$
 (1)

Where O_2 ' is the expected oxygen in μ mol L^{-1} at equilibrium with the atmosphere, at the measured temperature and salinity according to Grasshoff et al., (1999), and O_2 is the oxygen concentration measured by the FerryBox optode.

Duran bottles (~ 300 mL) were filled with sample water during all seasonal cruises using the FerryBox outflow to measure turbidity and salinity in the laboratory. Salinity was measured using an OPTIMARE High Precision Salinometer (Optimare Systems GmbH, Bremerhaven, Germany) and turbidity was measured using a Hach 2100 turbidimeter.

Nutrient samples were collected at each station using the onboard water sampler. A sample volume of 250 ml was filtered through pre-combusted GF/F filters, and the samples were collected in clean centrifuged tubes, frozen and stored at -20 °C. The concentrations of nitrite (NO_2^-), nitrate (NO_3^-) ammonium (NH_4^+) and silicate (SiO_2) were also measured using a MicroMaC analyser from SYSTEA (Anagni (FR), Italy). The system, which induces a colour reaction, is coupled with a photometer (NO_2^- , NO_3^- , SiO_2) and a fluorometer (NH_4^+), using a one-point calibration. NO_3^- was determined with sulfanilamide and N- (1- Naphthyl)ethylenediamine, NH_4^+ with orthophthalaldehyde and NO_2^- with diethylenetriaminepentaacetic acid and automatic UV reduction (Luitjens, 2019).

Water samples for TA and DIC were collected in 300 mL BOD bottles at all stations using the FerryBox outflow according to the Standard Operating Procedure (SOP) (Dickson et al. 2007). The samples were poisoned with saturated mercury chloride and measured in the laboratory with a VINDTA 3C (MARIANDA, Kiel, Germany), using certified reference material (CRM) (Dickson et al. 2003). The results within this study were plotted with R Project (ggplot package) and maps were created with ArcGIS Pro. In addition, the saturation state of calcite (Ωcal) calculated using the CO2SYS program developed by (Lewis et al. 1998) with CO₂ solubility constants of Lueker et al. (2000).

2.4 [TA-DIC] as a proxy for Biogeochemical Processes

145 [TA-DIC] is a good proxy for biogeochemical processes such as CaCO₃ precipitation / formation, photosynthesis, respiration and therefore CO₂ uptake and release, even in coastal oceans (Xue and Cai, 2020). The parameter is independent of ocean mixing and not sensitive to temperature and pressure changes, and this makes it a good tracer for larger-scale oceanographic studies, and suitable for seasonal observations of biogeochemical processes and carbonate dynamics of an ecosystem. In addition, it is assumed that [TA-DIC], can better reflect variations of [CO₃²⁻] compared to the ratio of TA and DIC (Xue et al., 2017).

The difference between TA and DIC is often expressed as:

$$[TA - DIC] = TA - DIC$$
 (2)

However, [TA–DIC] should not be used at low salinity (e.g. <20) and when [TA–DIC] is $< 50 \,\mu$ mol kg⁻¹, where the relationships of [TA–DIC] with pH and/or ocean acidification are nonlinear, these low values also occur in oxygen minimum zones (Xue and Cai 2020).

2.5 Calculations of estuarine DIC and TA contributions

155

160

To estimate the contributions of estuarine DIC and TA in the Western and Eastern EFWS, we used DIC measurements from the lowest salinity station in the Estuary where the Ems enters the Wadden Sea as endmembers for our mixing model. The stations chosen for these measurements were in areas of low salinity within the estuary, with considerable influence of freshwater (Table 1). These values (DIC_{estuary}; TA_{estuary}) were used to calculate the DIC_{mixing w/R} and TA_{mixing w/R} (equation 3; 4) for the different regions.

Table 1: DICestuary, DICNorthSea, SNorthSea, TAestuary and TANorthSea used for the calculation of the seasonal DICmixing w/R concentrations of each season.

Season and Region	DICNorthSea	DICestuary	SNorthSea	TANorthSea	TAestuary
July 2021	2144.07	2261.20	31.79	2273.70	2465.12
October 2021	2188.46	2224.90	30.97	2369.27	2411.68
March 2022	2205.66	2238.05	31.47	2338.37	2318.90
May 2022	2199.86	2205.52	32.13	2332.49	2447.76
July 2022	2144.41	2310.22	31.78	2356.59	2489.56

In this study, DIC_{NorthSea} (and TA_{NorthSea}) refers to the DIC (and TA) values at the station (CAR_S_076) located farthest from land behind Spiekeroog and Wangeoog (Fig. 1b), which we used as our marine endmember, as it is situated farthest offshore of the Ems and experiences the highest salinity (S_{NorthSea}) levels during almost each season. The DIC_{NorthSea} and TA_{NorthSea} endmembers applied for each season are shown in Table 1.

Starting with these endmembers, we used the equations of Jiang et al. (2008) and Joesoef et al. (2015) to calculate the contribution of riverine DIC and TA:

170
$$\operatorname{DIC}_{\operatorname{mixing w/R}} = \frac{S_i}{S_{\operatorname{NorthSea}}} * \operatorname{DIC}_{\operatorname{NorthSea}} + (1 - \frac{S_i}{S_{\operatorname{NorthSea}}}) * \operatorname{DIC}_{\operatorname{estuary}}$$
 (3)

$$TA_{\text{mixing w/R}} = \frac{s_i}{s_{\text{NorthSea}}} * TA_{\text{NorthSea}} + (1 - \frac{s_i}{s_{\text{NorthSea}}}) * TA_{\text{estuary}}$$
(4)

where S_i represents the salinity at each related station *i*. The ratio $\frac{S_i}{S_{NorthSea}}$ normalizes the influence of the salinity at the specific station by the salinity of the North Sea ($S_{NorthSea}$).

In addition, the ΔDIC_{excess} was calculated to estimate the contribution due to estuarine input in the different regions. Therefore,

the equation of (Jiang et al., 2008; Van Dam et al., 2018) was used:

185

190

$$\Delta DIC_{\text{excess}} = DIC_i - DIC_{\text{mixing w/R}}$$
(5)

This equation includes the measured DIC concentrations of the related station i and the DIC_{mixing w/R}.of equation 3. $\Delta TA_{mixing w/R}$.and ΔTA_{excess} were calculated the same way with the measured TA of each station using the $TA_{extuary}$, $TA_{NorthSea}$ values (Table 1):

$$180 \quad \Delta T A_{\text{excess}} = T A_i - T A_{\text{mixing w/R}} \tag{6}$$

 ΔDIC_{excess} and ΔTA_{excess} concentrations were calculated to remove the mixing effect of water masses from the estuary outflow with the North Sea, as the coastal region of the EFWS is closely connected to the land. A ΔDIC_{excess} value of approximately zero means that the DIC is not different than what would be expected from mixing between the North Sea and estuarine outflow waters. Negative values of ΔDIC_{excess} indicate that the DIC consumption exceeded production in this area, which reduces DIC or, equivalently increases ΔTA_{excess} . Positive values of ΔTA_{excess} suggests higher values than expected based on mixing alone, indicating TA sources.

Therefore, during productive seasons, primary production will decrease DIC, while consuming CO_2 and nutrients (Xue and Cai, 2020). The uptake of NO_3^- can increase TA, while the uptake of NH_4^+ can decrease TA in an ecosystem (Brewer and Goldman, 1976; Wolf-Gladrow et al., 2007). The production of 1 mol organic matter ($(CH_2O)_{106}(NH_3)_{16}H_3PO_4$) will generally increase TA by 17 mol TA (ΔTA_P) and decrease DIC by 106 mol and will change the TA and DIC concentrations (Chen, 1978). Consequently, ΔTA_P is used to calculate the expected amount of TA produced, according to the equation of ΔTA_{bio} from (Xue and Cai 2020), which was modified using the calculated ΔDIC_{excess} :

$$\Delta T A_P = -17/106 * \Delta DIC_{excess} \tag{7}$$

It is important to note, that the calculation of ΔTA_P is an overestimation assuming the measured TA is modulated by photosynthesis (NO₃⁻ - fueled) or respiration, such that the presence of other non-photosynthetic DIC sinks will cause ΔTA_P to be overestimated.

3 Results

215

220

3.1 Regional and seasonal variation in the EFWS

In July 2021, salinities were lowest on the route from Norddeich harbour to Norderney (25.2), and around Norderney (Table 2; Fig. S1) in the Western WS. In summer 2022, the salinity on July 12 (31.16 - 32.03) increased by 2 - 3 salinity units compared to July 11 (28.28 - 29.43) in the Eastern WS (Table 2; Fig. S1). This indicates that during July 2022 cruise, there was a change in salinity range between the first and second leg of the cruise (in roughly the same region). A possible reason for these salinity differences could be the Neuharlingersiel sluice opening in the early morning of July 11, 2022, which could have influenced the salinity on this day. The turbidity in October 2021 showed a completely different pattern compared to all other seasons, with values from 96.08 – 306.46 NTU (Fig. S1), caused by rougher weather conditions during the campaign.

A land to sea gradient was observed in pH in October 2021 (Fig. S2), which varied from 7.6 to 8.1 (Table 2). Higher values were measured in the North Sea regions (behind Juist, Norderney, Langeoog), whereas the lower values were measured closer to the mainland. Regional differences with maximum pH values of > 8 in the higher salinity waters were measured during all seasons (Fig. S2; Table 2), with pH > 8 in the Western WS, in front of Norderney in May 2022.

210 Table 2: Overview of the different measured parameters: Temperature (°C), Salinity, pH, oxygen (% saturation), AOU (μmol L⁻¹), Chlorophyll a (Chl a in μg L⁻¹), pCO_{2 obs} (μatm) and Calcite saturation Ωcal of all seasonal samplings in the EFWS.

Parameter	July 2021	October 2021	March 2022	May 2022	July 2022
Temperature (°C)	18.59 – 23.15	12.66 – 16.57	3.89 - 6.47	9.65 – 18.19	17.36 - 21.04
Salinity	25.21 – 32.33	25.21 – 31.32	18.32 – 31.97	23.59 – 32.28	23.35 - 32.04
pН	7.71 – 8.16	7.64 - 8.13	7.66 – 8.13	7.95 - 8.55	7.71 - 8.08
Oxygen (% sat)	109.7 ± 9.5	100.9 ± 5.3	105.5 ± 3.1	132.9 ± 13.0	102.4 ± 5.2
AOU (µmol L-1)	-22.7 ± 22.2	-2.3 ± 14.4	-17.5 ± 10.0	-88.9 ± 33.9	-5.3 ± 12.4
Chl a (µg L ⁻¹)	25.6 ± 12.9	16.9 ± 8.9	13.4 ± 6.5	52.1 ± 29.4	23.2 ± 19.3
pCO _{2 obs} (µatm)	-	521.6 ± 72.2	468.2 ± 54.5	269.0 ± 63.7	536.0 ± 116.5
Ωcal	3.8 ± 0.9	3.21 ± 0.6	2.5 ± 0.4	5.2 ± 1.1	3.7 ± 0.4

The maximum concentrations of chlorophyll a were observed in May 2022, displaying the most substantial fluctuations (Table 2), especially in the Western part from Norderney to Borkum (up to 151.7 μ g L⁻¹) (Fig. S2). In July 2021, the highest chlorophyll measurements (up to 74.7 μ g L⁻¹) were detected underway between Norderney to Spiekeroog (Table 2; Fig. S2). A similar pattern can be seen for July 2022 (Fig. S2), however no measurements from Norderney to Spiekeroog are available

A similar pattern can be seen for July 2022 (Fig. S2), however no measurements from Norderney to Spiekeroog are available for chlorophyll a. This is also the case for October 2021 from Norderney to Wangeoog (Fig. S2).

In July 2021 the measured oxygen ranged from 72.4 - 112.01 in % saturation (Fig. S2), with the highest values in the Wadden Sea of Langeoog. Oxygen decreased from July 2021 to October 2021, on average by 8.8 ± 10.9 % saturation (Table 2; Fig. S2). The lowest oxygen saturation was measured from Norddeich to Norderney in October (down to ~ 57 % saturation). Until May, oxygen saturation increased continuously over the year. The highest oxygen (up to ~ 180 % saturation) was measured in May in the intertidal region of Norderney in the Western and around Wangeoog in the Eastern EFWS (up to ~ 152 % saturation)

(Table 2; Fig. S2). Overall, oxygen decreased by a mean value of 28.4 ± 16.4 % saturation from May to July 2022 (Fig. S2), resulting in slightly lower oxygen saturation in July 2022 compared to the previous year (Table 2). For the AOU (Table 2), the same inverse picture was obtained. The observed pCO_2 (pCO_2 obs) was highest in July 2022 and lowest in May 2022 (down to 141.3 µatm) in the Western WS. The average decrease in pCO_2 obs was 166.2 ± 276.1 µatm from March to May 2022 (Table 2; Fig. S3).

During all seasons, Ω cal was supersaturated, ranging from 1.5 – 7.5 (Table 2), but with a pronounced seasonal pattern. Higher, supersaturated Ω cal values (> 2.5) were observed during more productive seasons (July 2021, July 2022, May 2022). However, the highest variability of Ω cal was found in May 2022 with values > 1 in 80 % of the stations and reaching up to 7.52 in the WS of Juist and Borkum (Table 2; Fig. S3). In summer (July 2021, July 2022), a decrease of Ω cal in the EFWS from West to East was observed, regionally (Fig. S3).

3.2 TA and DIC Variability in the EFWS

225

230

235

240

Large variability in DIC and TA was observed, seasonally but also regionally along the land to sea gradient in the EFWS (Table 3; Fig. 2) with high TA in summer (Fig. 2). In July 2021, TA ranged from ~ 2273 μmol kg⁻¹ in the Jade Bay (Eastern WS) and increased regionally westward (up to ~ 2465 μmol kg⁻¹) to Norderney (Table 3; Fig. 2; Fig. 3a). All measured TA values were above or slightly below the mixing line with a negative slope (- 24.9 μmol kg⁻¹ per salinity unit) (Fig. 3a), indicating TA production. In July 2022, lower TA values were measured during the first leg of the cruise when salinities were lower (28 - 29) (Table 3; Fig. 2; Fig. 3a), but a similar slope (- 23.3 μmol kg⁻¹ per salinity unit) of the short mixing line was observed (Fig. 3a). At higher salinity stations in July 2022 (up to 32), TA values were similar to those measured the previous summer, with a negative slope of -25.1 μmol kg⁻¹ per salinity unit, slightly above the mixing line, indicating TA production (Fig. 3a). The DIC concentrations also showed a similar pattern during both summer cruises (Table 3; Fig. 3b), with negative slopes of -49.0 μmol kg⁻¹ and -44.3 μmol kg⁻¹ per salinity unit in July 2021 and 2022, respectively, in the Eastern WS.

Table 3: Overview of different the parameters TA (μ mol kg⁻¹), DIC (μ mol kg⁻¹) and [TA-DIC] (μ mol kg⁻¹) of all seasonal samplings in average with the standard deviation.

Parameter	July 2021	October 2021	March 2022	May 2022	July 2022
TA (μmol kg ⁻¹)					
Western WS	2403.4 ± 27.4	2388.6 ± 15.6	2358.6 ± 27.8	2378.9 ± 39.0	2380.2 ± 42.7
Eastern WS	2283.5 ± 10.2	2236.6 ± 5.3	2347.2 ± 11.8	2349.7 ± 9.8	2337.2 ± 35.2
DIC (μmol kg ⁻¹)					
Western WS	2185.8 ± 48.2	2257.1 ± 91.0	2237.7 ± 37.8	2065.5 ± 107.0	2184.4 ± 43.3
Eastern WS	2124.1 ± 10.3	2182.8 ± 18.2	2211.8 ± 20.9	2089.2 ± 38.0	2142.3 ± 27.6
[TA-DIC]					
(µmol kg ⁻¹)					
Western WS	217.55 ± 51.9	150.5 ± 47.1	120.9 ± 30.2	313.3 ± 76.1	196.8 ± 26.7
Eastern WS	159.44 ± 16.4	184.9 ± 19.9	137.9 ± 11.0	260.5 ± 34.7	194.9 ± 21.1

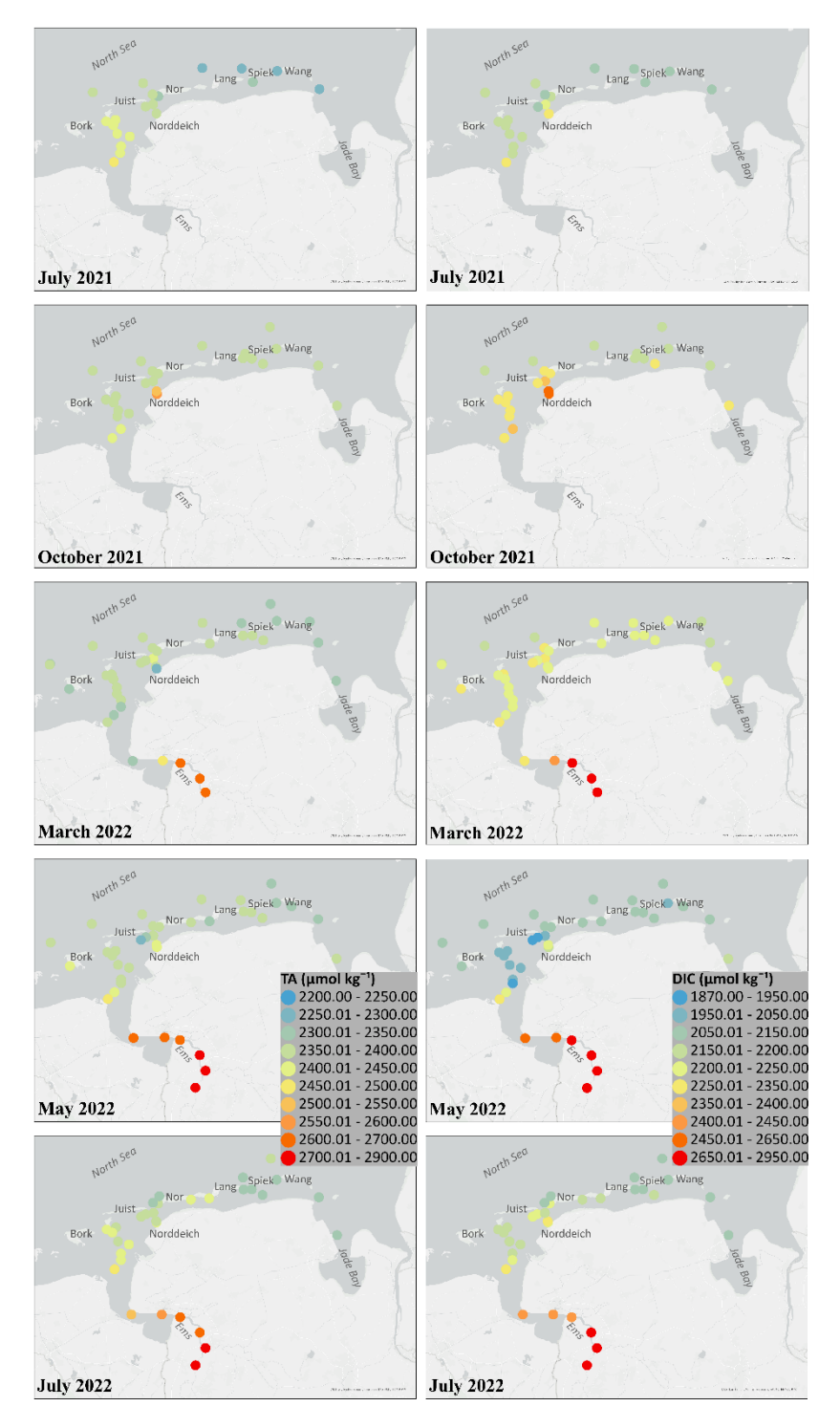
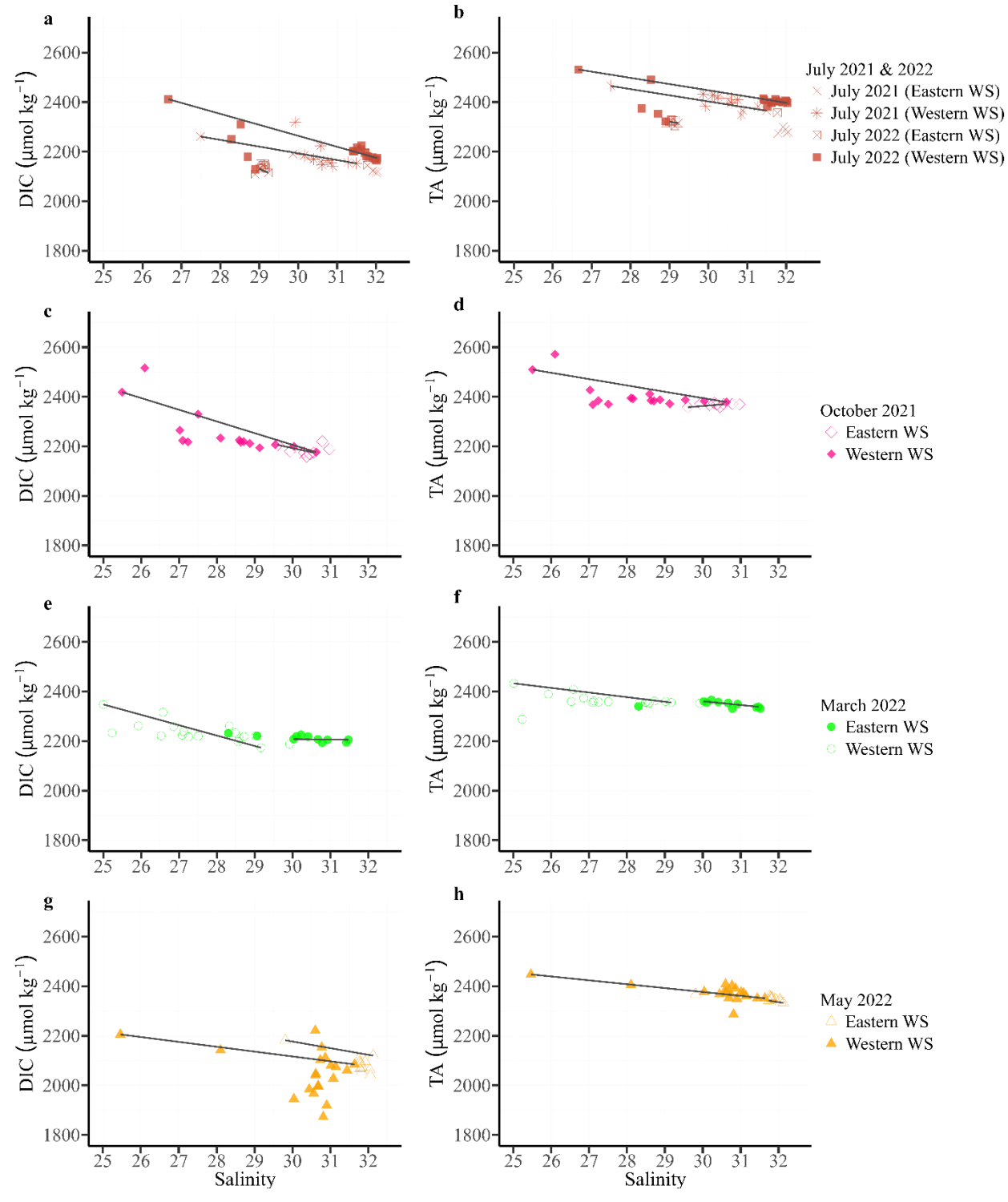


Figure 2: Measured results of TA and DIC of all seasonal cruises of July 2021, October 2021, March 2022, May 2022 and July 2022. All TA and DIC values are in μmol kg ⁻¹). The map in this Figure was generated using ArcGIS. Data sources: LGLN, Esri, TomTom, Garmin, Foursquare, FAO, METI/NASA, USGS. © 2024 Julia Meyer.



250 Figure 3: TA (μmol kg⁻¹) and DIC (μmol kg⁻¹) mixing plots, against salinity of July 2021 (a, b), October 2021 (c, d), March 2022 (e, f), May 2022 and July 2022 (a, b) at > 25 salinity, separated by the different regions (Eastern WS, Western WS) of the EFWS.

In October 2021, the highest TA concentrations were measured at a station near Norddeich (up to 2571 μmol kg⁻¹) in the Western WS (Fig. 2). The DIC values reached a maximum of 2516 μmol kg⁻¹ in front of Norderney and decreased with increasing longitude to a minimum of 2158 μmol kg⁻¹ (Fig. 2). The mixing plot of TA in October 2021 shows a negative mixing line in the Western WS (- 25.4 μmol kg⁻¹ per salinity unit), whereas the Eastern WS shows an almost linear mixing line with a positive slope of 13.1 μmol kg⁻¹ per salinity unit (Fig. 2; Fig. 3c). A similar picture of TA was observed in the Western WS (- 46.9 mol kg⁻¹ per salinity unit) (Fig. 3d). In March 2022, lower DIC concentrations (< 2200 μmol kg⁻¹) were measured further offshore behind the islands of Borkum, Juist and Norderney, which increased slightly closer to land (Fig. 2). The mean measured TA in the Western WS in May was 2378.9 μmol kg⁻¹ (Table 3, Fig. 2), indicating a slight increase in TA from March to May 2022. Most of the TA values were close to or above the mixing line, with similar negative slopes in the Western (- 15.6 μmol kg⁻¹ per salinity unit) and in the Eastern WS (- 15.3 μmol kg⁻¹ per salinity unit) (Fig. 3g). The lowest DIC values (down to 1872 μmol kg⁻¹) in this study were also measured in the Western WS in spring (Table 3; Fig. 2; Fig. 3h).

3.3 Seasonal Trends in [TA-DIC] and AOU in the EFWS

255

260

275

The relationship between [TA–DIC] and AOU provides valuable insights into the biogeochemical processes that drive carbonate dynamics in coastal systems (Xue and Cai, 2020). A critical threshold for interpreting this relationship is that [TA–DIC] cannot be used when values are < 50 µmol kg⁻¹, as proposed by Xue and Cai (2020). This threshold applied only to one station near Norddeich harbor in October (Fig. 7), so these data were excluded from the seasonal calculations (Table 3).

Figure 4a illustrates the AOU relationship to [TA-DIC] from all stations sampled during various seasons in the Wadden Sea.

The regression analysis highlights a negative correlation, with a slope of -1.416 μmol kg⁻¹ per μmol L⁻¹ of AOU, which is steeper than the Redfield ratio slope (- 123/138 = -0.89), previously proposed by Xue and Cai (2020). In spring, negative AOU values (down to -169 μmol L⁻¹, Fig. 4a) were observed alongside higher [TA-DIC] values (> 200 μmol kg⁻¹; Fig. 4b).

In the summer (2021; 2022), [TA-DIC] values from the Eastern WS are located under the respiration/photosynthesis line ($< 200 \,\mu\text{mol kg}^{-1}$; Fig. 4b). In contrast, the measured [TA-DIC] concentrations in the Western WS in summer are $> 200 \,\mu\text{mol kg}^{-1}$, above the respiration/photosynthesis fit (Fig. 4b). In July 2022, the salinity in the same region changed by 2 - 3 units from one day (July 11) to another (July 12), where the salinity was higher in the East, showing slightly higher TA values ($+53.7 \pm 36.7 \,\mu\text{mol kg}^{-1}$) in summer 2022, compared to the previous year (Table 3).

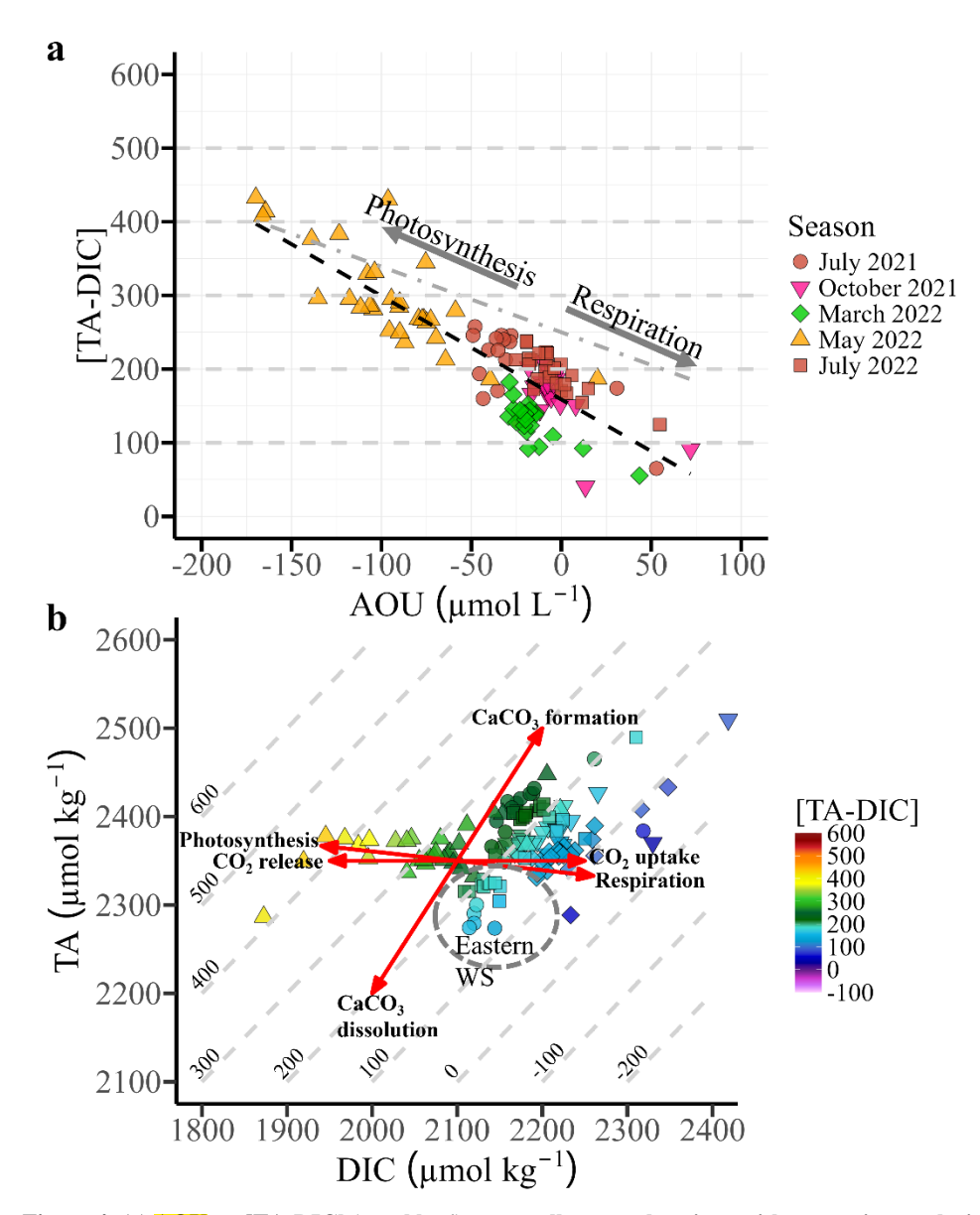


Figure 4: (a) AOU vs. [TA-DIC] (μmol kg⁻¹) across all seasonal cruises, with regression analysis (black dashed line). Arrows indicate potential processes affecting [TA-DIC] and apparent oxygen utilization (AOU). The grey dashed line represents the regression slope (-123 / 138 = -0.89) proposed by Xue and Cai (2020). (b) DIC versus TA plot from all seasons, with the coloured values of [TA-DIC] for the EFWS at salinity 25 – 32.5. Isoclines represent [TA-DIC] values. Red lines indicate key biogeochemical processes (photosynthesis / respiration, CO₂ exchange, and CaCO₃ formation / dissolution). The Eastern EFWS is highlighted with a grey circle.

3.4 Seasonal Variability of DIC and TA in the EFWS: Influence of Mixing Processes

285

Stations located near Norddeich harbour, closer to the mainland, exhibit extreme values (Fig. 2) and therefore were excluded from the calculation of mean \pm standard deviation to provide a more representative assessment of ΔDIC_{excess} , ΔTA_{excess} , and

 ΔTA_P . However, these values are still displayed in the scatter plots (Fig. 5) to illustrate the range of variability, including highly positive and negative deviations.

The Western WS generally exhibits positive ΔDIC_{excess} values, with a peak in October 2021 (47.7 ± 84.9 µmol kg⁻¹) and July 2022 (54.6 ± 33.3 µmol kg⁻¹), suggesting an excess of DIC beyond the expected mixing (Fig. 5a). In contrast, during May, ΔDIC_{excess} in the Western WS was negative (-69.3 ± 107.0 µmol kg⁻¹), suggesting significant DIC consumption, potentially due to enhanced primary production during spring bloom conditions. Similarly, negative values were observed in the Eastern WS in May 2022 (-30.1 ± 35.8 µmol kg⁻¹) and July 2021 (-19.3 ± 11.2 µmol kg⁻¹) (Table 4; Fig. 5a).

Higher ΔTA_{excess} values are observed in the Western WS, particularly in July 2021 (123.0 ± 27.8 μmol kg⁻¹), indicating additional alkalinity sources. In spring, ΔTA_{excess} showed a clear positive trend, with an increase from March to May in both regions (Fig. 5b), suggesting that while TA is being consumed, production still exceeds consumption. The increases in TA from March to May were 20.0 ± 42.22 μmol kg⁻¹ in the Western WS and 8.1 ± 18.62 μmol kg⁻¹ in the Eastern WS (Table 4; Fig. 5). The Eastern WS exhibits lower ΔTA_{excess} values, with some negative values in July 2022 (-34.7 ± 32.3 μmol kg⁻¹), when the sluice was open. ΔTA_P, representing primary production effects, is positive in May (Table 4; Fig. 5c) in the Western and Eastern WS, indicating a net uptake of CO₂ through biological processes and a corresponding decrease in DIC (Fig. 5a).

Table 4: Mean ± Standard Deviation of ΔDIC_{excess}, ΔTA_{excess}, and ΔTA_P (μmol kg⁻¹) of all seasons in the Eastern and Western EFWS.

Season	July 2021	October 2021	March 2022	May 2022	July 2022
ΔDIC _{excess}					
Western WS:	23.4 ± 27.6	47.7 ± 84.9	20.5 ± 23.8	-69.3 ± 107.0	54.6 ± 33.3
Eastern WS:	-19.3 ± 11.2	-6.37 ± 19.4	5.85 ± 11.2	-30.1 ± 35.8	-16.0 ± 26.2
ΔTAexcess					
Western WS:	123.0 ± 27.8	29.9 ± 51.9	16.6 ± 21.9	36.6 ± 36.1	50.9 ± 21.9
Eastern WS:	10.9 ± 11.5	-2.35 ± 5.87	10.7 ± 12.5	18.8 ± 13.8	-34.7 ± 32.3
ΔΤΑΡ					
Western WS:	-3.75 ± 4.43	-7.65 ± 13.6	-3.28 ± 3.82	11.1 ± 17.2	-8.75 ± 5.35
Eastern WS:	3.10 ± 1.80	1.02 ± 3.11	-0.845 ± 1.72	4.83 ± 5.74	2.56 ± 4.20

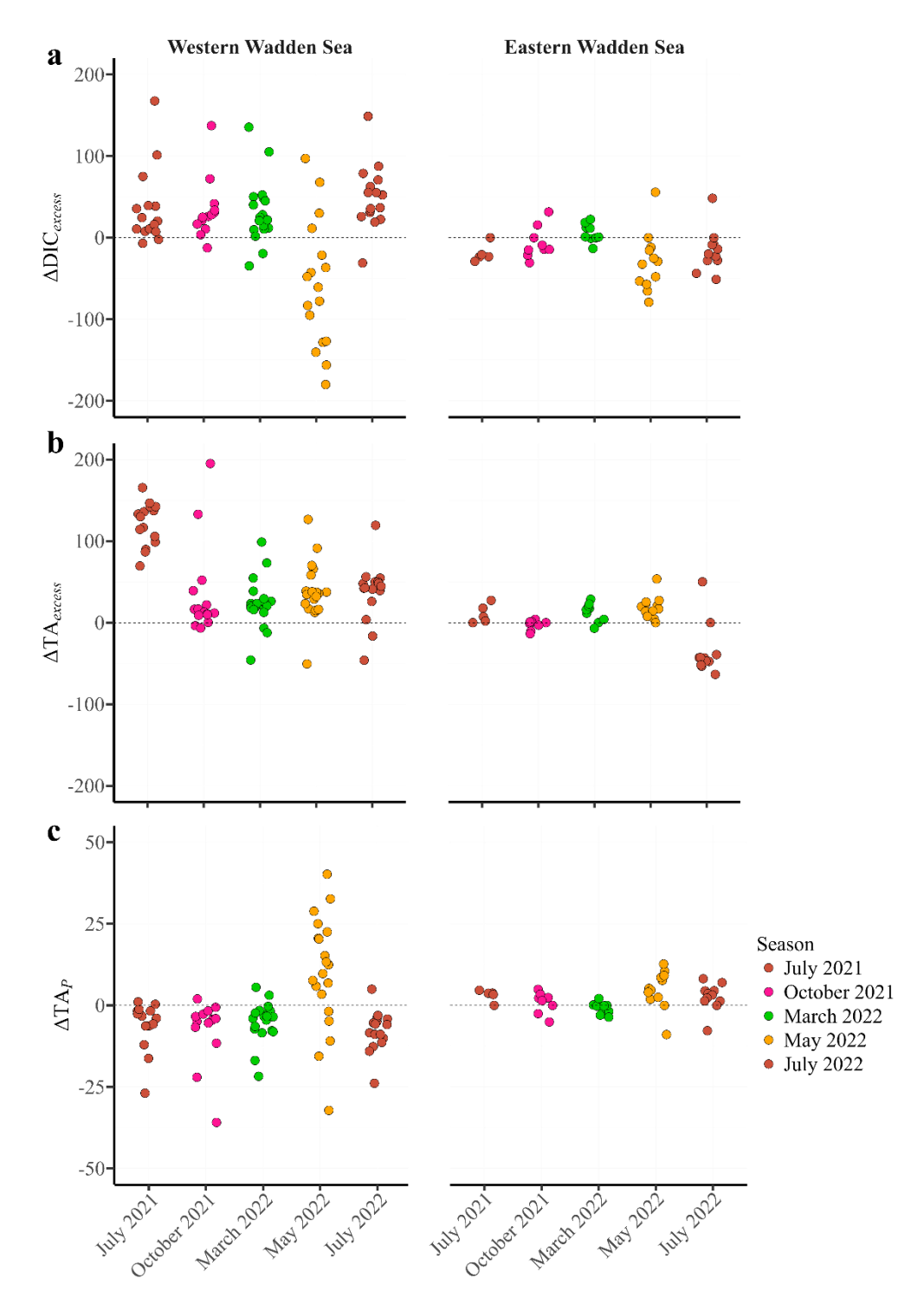


Figure 5: The scatter plots illustrate the seasonal variations of ΔDIC_{excess} , (a) ΔTA_{excess} , (b) and ΔTA_{P} (c) in μ mol kg⁻¹ in the Western WS (left panels) and Eastern WS (right panels) from each season. Each colour represents different seasons.

3.5 Regional and seasonal variation of Nutrients

310

315

320

A clear seasonal pattern can also be seen in the measured nutrients (Fig. S4). For NO_2^- and NH_4^+ a decrease in concentrations was observed from October 2021 to May 2022, except in the East part of the EFWS (Fig. S4), where the concentration did not change much. NO_3^- concentration ranged seasonally, with an increasing trend from summer to March 2022 (up to 66.28 μ mol L^{-1}) in the EFWS. In May 2022, the NO_3^- concentrations decreased again below the detection limit of the instrument (> 0.01 μ mol L^{-1}) at some stations, mainly in the Western part (Fig. S4). This analogous seasonal tendency possibly will point to common sources and sinks.

Overall, from March 2022 to May 2022 there was an average decrease in NO_3^- of 19.29 ± 18.11 µmol kg⁻¹ (Fig. 6). TA slightly increased by 9.1 ± 29.2 µmol kg⁻¹ during this time (Fig. 4 - 6), while DIC decreased on average by 159.4 ± 125.4 µmol kg⁻¹. The differences of NO_3^- and SiO_2 for all stations between March and May 2022 (ΔNO_3^- , ΔSiO_2) were plotted against the DIC difference between March and May (ΔDIC , Fig. 6). For ΔNO_3^- a regression line was fitted with equation of y = 6.90x + 29.089 ($R^2 = 0.4637$, p- value = < 0.05, Fig. 6), while the ΔSiO_2 regression has an equation of y = 8.11x + 50.605 ($R^2 = 0.2165$, p- value = < 0.05; Fig. 6). The slope of both regression lines is close to the Redfield Ratio (Redfield et al., 1963) of 106/16 = 6.625 for NO_3^- (6.90, Fig. 6) and 106/15 = 7.067 for SiO_2 (8.11, Fig. 6), indicating that the identified enhanced primary production in this region in spring, along with nutrient (nitrate) uptake most likely lead to a concomitant decrease in DIC (Fig. 6) and increase TA.

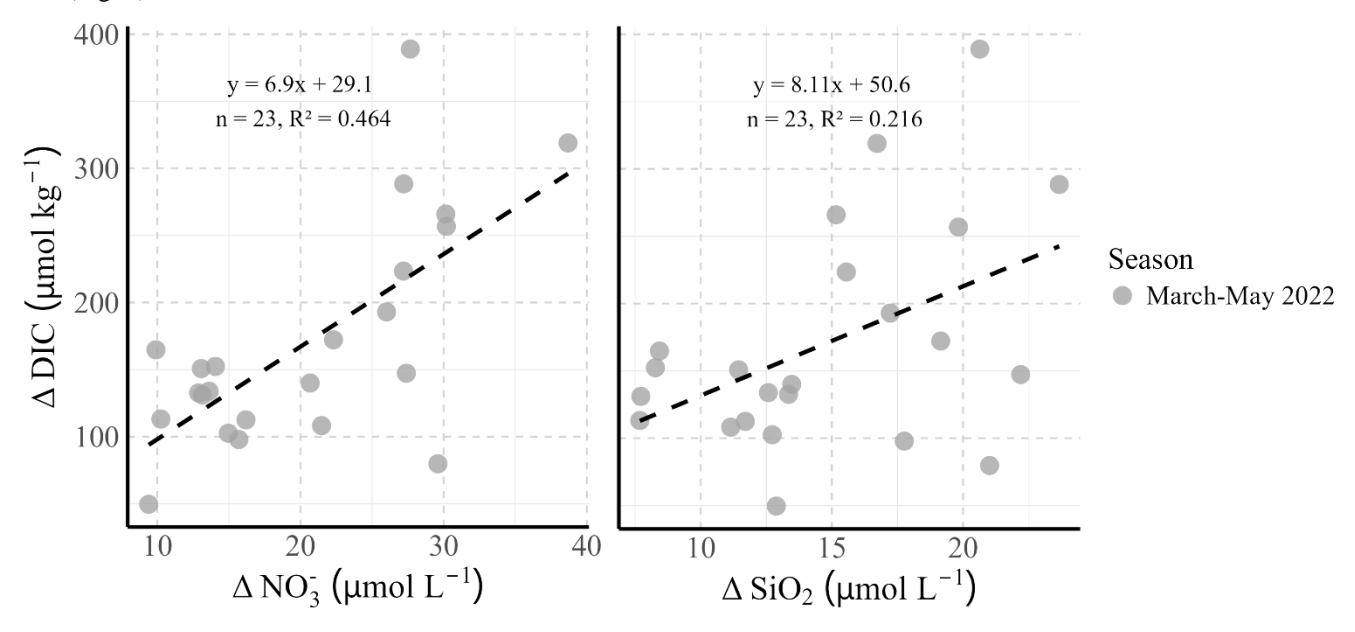


Figure 6: NO_3 and SiO_2 differences (ΔNO_3 , ΔSiO_2) of March to May 2022 against the difference of DIC (ΔDIC), with the related regression equations. The slopes show the Redfield Ratios of all measured stations in the Western and Eastern WS.

Discussion

4.1 Regional and seasonal Differences of the Carbonate Dynamics in the EFWS

This study highlights regional and seasonal variability in the carbonate system, with a notable West-to-East gradient in DIC and TA, showing considerable fluctuations across seasons (Table 3; Fig. 2). This is the first study to investigate ΔDIC_{excess}, ΔTA_{excess}, ΔTA_P [TA-DIC] in the EFWS to provide insights into the respective biogeochemical processes and to determine the source and sink dynamics of carbon on such a large spatial and temporal scale (Table 4; Fig. 5). We successfully demonstrated that TA increased in the spring because of intense primary production, most likely driven by nitrate uptake (Figs. 5; Fig. 6), highlighting the impact of biological activity on carbonate system dynamics. During the other seasons, the system acted as a source of DIC, indicating seasonal shifts in carbon cycling. Similar patterns of intense production periods and TA increases have also been reported in the North Sea adjacent to the Wadden Sea (Voynova et al., 2019). Additionally, we observed TA production during summer, which was more prominent in the Western WS, further suggesting that these intertidal regions act as a stronger source of TA and DIC during all seasons except in spring, compared to the Eastern EFWS.

4.2 Seasonal TA Production and DIC Dynamics in the EFWS

The data reveal important differences in the patterns between years and regions in summer (Table 4; Fig. 2 – 5). The observed summer dynamics in the Eastern and Western EFWS show distinct patterns in the biogeochemical processes related to TA and DIC production. Positive ΔTA_{excess} (e.g., $123.0 \pm 27.8 \mu mol \ kg^{-1}$ in July 2021) and ΔDIC_{excess} (23.4 \pm 27.6; Table 4) values suggest that there is excess of TA and DIC in the Western EFWS. One key biogeochemical process, which can contribute to increasing TA, without a proportional increase in DIC, is the dissolution of CaCO₃, which results in elevated [TA-DIC] values (>200 μ mol \kg^{-1}) (Chen and Wang, 1999; Hoppema, 1990). However, CaCO₃ dissolution can be ruled out as a major TA source in the water column, since calcite is supersaturated (Ω cal > 1) during the study period (Brasse et al., 1999; Norbisrath et al., 2024). Nevertheless, in the sediments large amount of DIC can be produced by carbonate shells and transported by erosion processes into the water column (Brasse et al., 1999). Previous studies have estimated that TA production in the Wadden Sea is driven by anaerobic processes such as denitrification and/or CaCO₃ dissolution in sediments (Norbisrath et al., 2024; Thomas et al., 2009). Anaerobic degradation of organic matter—via denitrification and sulfate reduction—releases both TA and DIC (Brasse et al., 1999; Hu and Cai, 2011; Norbisrath et al., 2024; Thomas et al., 2009), with TA concentrations reaching up to 2310 μ mol \kg^{-1} in summer (Thomas et al., 2009). Other studies suggest that permeable Janssand sediments (a tidal sand flat in the back-barrier area of Spiekeroog Island, Eastern EFWS) exhibit the highest potential denitrification rates (Gao et al., 2010).

In the summer months, the production of TA in both the Eastern and Western EFWS can be attributed to the decomposition of organic matter, especially following a productive spring season, such as the one observed in May 2022 (see section 4.3), which likely led to an elevated input of organic matter into the system (Borges et al., 2017). This organic matter subsequently undergoes both aerobic and anaerobic decomposition in the sediments during the summer months, where anaerobic processes

like denitrification and sulphate reduction are drivers in generating both TA and DIC (Brasse et al., 1999; Norbisrath et al., 2024). These processes can significantly contribute to the enhancement of TA production (Fig. 4a, b; Fig. 5b), especially in the Western EFWS, where sedimentary anaerobic processes dominate in the summer (Al-Raei et al., 2009; Böttcher et al., 1998; Hu and Cai, 2011; Kamyshny and Ferdelman, 2010; Norbisrath et al., 2024; Thomas et al., 2009; Wu et al., 2015). Furthermore, with oxygen saturation remaining high (> 100 % saturation) and apparent oxygen utilization (AOU) being negative (Fig. 4a), it is evident that the water column is net autotrophic. This suggests that TA is primarily produced in the sediments and subsequently transported into the water column, rather than being generated in situ via remineralization (Beck and Brumsack, 2012; Postma, 1981).

365 Organic matter remineralization varies regionally across the North Frisian Wadden Sea (NFWS), EFWS, and Jade Bay (Van Beusekom et al., 2012; Kowalski et al., 2013). The NFWS favours aerobic degradation due to its wide tidal basins and highwater exchange (~8.1 km³ d⁻¹), resulting in lower organic matter accumulation, reduced eutrophication, and lower TA production relative to DIC (Van Beusekom et al., 2012; Kowalski et al., 2013; Schwichtenberg et al., 2020). In contrast, the EFWS experiences higher eutrophication and organic matter accumulation due to its narrower basins and limited exchange, 370 promoting anaerobic degradation processes (e.g., sulfate reduction), which enhance TA production (Van Beusekom et al., 2012; Kowalski et al., 2013; Schwichtenberg et al., 2020; Thomas et al., 2009). Jade Bay, with the lowest water exchange (~0.8 km³ d⁻¹), exhibits sporadic high TA/DIC ratios, likely due to short-term iron reduction processes (Brasse et al., 1999). A similar pattern was also seen in the Eastern EFWS compared to the Western in [TA-DIC] dynamics (Fig. 2; Fig. 4b). In comparison to the Western, the Eastern EFWS consistently exhibits lower [TA-DIC] values (<200 µmol kg⁻¹) during the 375 summer months of 2021 and 2022, while the Western EFWS shows slightly higher [TA-DIC] values (>200 µmol kg⁻¹; Fig. 4b). This difference can be attributed to enhanced CaCO₃ formation, as indicated by its Ω cal (1.9 \pm 0.8) in the Eastern (Fig. 4b). CaCO₃ formation likely consumes TA (Chen, 1978), leading to the observed shift toward negative $\Delta TA_{\text{excess}}$ values (Fig. 5b). The formation of CaCO₃, particularly in sediments or shells, contributes to the lower observed source of TA in the Eastern compared to the Western WS. Despite this, the region still acts as a net source of TA, which aligns with the assumption that 380 the Eastern EFWS can contribute TA to the coastal system during the summer months, especially from anaerobic degradation

Additionally, the salinity change observed in July 2022 was likely due to local anthropogenic influences, such as the sluice opening in summer 2022. On July 11, 2022, the sluice in Neuharlingersiel was opened just before we started our sampling. This anthropogenic intervention likely caused sudden changes in salinity and local hydrological conditions (Fig. S1; Fig. 3a, b), making it reasonable to treat the July 11 measurements as anomalous. It is important to note that the lower [TA-DIC] values in the Eastern EFWS are observed both on the day of sluice opening in July 2022 and on the day when the sluice was closed in July 2021. This suggests that the impact of the sluice opening did not have a major impact on the overall [TA-DIC] dynamics in the region.

processes (Schwichtenberg et al., 2020; Thomas et al., 2009).

385

390

These seasonal shifts in TA can influence the coastal ocean's ability to absorb carbon from the atmosphere (Burt et al., 2016; Gruber et al., 2019; Li et al., 2024; Schwichtenberg et al., 2020). In summer, the generation of TA and DIC may alter the

region's buffering capacity, with the Western WS possibly storing or taking up carbon (Fig. 7) (Gruber et al., 2019; Li et al., 2024). These findings align with previous studies (Thomas et al., 2009; Voynova et al., 2019) suggesting that the intertidal regions of the EFWS act as a source of both TA and DIC to the coastal system during the summer months.

Particularly, the tidal WS plays an important role in the biogeochemical cycling of the North Sea (Santos et al., 2015; Thomas 395 et al., 2009), because many European rivers empty in the WS (Thomas et al., 2009). A few studies discussed the generation in of TA in summer before (Schwichtenberg, 2013; Voynova et al., 2019), however in summer the riverine inflow is lowest, which could not explain an increase of TA in the WS. The highest riverine contribution of TA is expected from January to April (Pätsch and Lenhart, 2004; Schwichtenberg, 2013). The moderate rainfall and cooler-than-average weather in October 2021 may have influenced the hydrology of the region, potentially causing increased terrestrial runoff and enhanced delivery 400 of alkalinity-rich water to the coastal system. The slight source of DIC in October (Table 3; Fig. 4d) suggests that organic matter remineralization and sediment-water exchange continue to play a role during this period (Borges et al., 2017). In addition, pore waters enriched with remineralized nutrients are actively released into the overlying water column (Beck and Brumsack, 2012) and organic matter-enriched water masses transported from the North Sea contribute to the availability of degradable material in the Wadden Sea, sustaining biogeochemical activity into autumn(Van Beusekom et al. 1999). This 405 mechanism aligns with studies highlighting the importance of tidal-driven nutrient and carbon fluxes in permeable sediments (Postma, 1981), where advective transport processes facilitate the continuous exchange of dissolved carbon species between sediments and the water column (Santos et al., 2015).

4.3 Nitrate Assimilation and Carbonate Dynamics in Spring

420

The highest rates of photosynthesis were measured in our study in the spring of 2022 (May 2022). This is evidenced by high O₂ levels (up to 180 % saturation), low *p*CO_{2 obs} (Table 2) and high chlorophyll a levels, along with negative AOU values (down to - 169 μmol L⁻¹; Fig. 4a) (Artioli et al., 2012; Thomas et al., 2005). These findings highlight the dominant role of photosynthetic activity in modulating the carbonate system, particularly in the Western EFWS, where carbon fixation via photosynthesis is a key factor in this study. The resulting changes in [TA-DIC] during this period are reflected in the AOU to [TA-DIC] relationship shown in Figure 4a, with a steeper negative slope of -1.416 μmol kg⁻¹ per μmol L⁻¹ AOU, deviating from the Redfield ratio of -0.89 (Xue and Cai, 2020). This deviation suggests that the EFWS may differ from the typical conditions assumed in the Redfield model (Redfield et al., 1963), which is primarily based on aerobic respiration and production (Xue and Cai, 2020).

Furthermore, [TA-DIC] increased due to the significant decrease in DIC in May 2022 (Fig. 4b). Together with the positive ΔTA_P and strongly negative ΔDIC_{excess} values after removal of mixing, this supports the findings of intense spring primary production generating TA, while drawing down DIC (Fig. 5). This was particularly evident in the Western EFWS, but also in the Eastern, indicating the Western EFWS is a stronger sink for CO_2 due to carbon fixation and nitrate assimilation (Borges et al., 2005). The May measurements follow roughly the photosynthesis/respiration line, indicated by the progressively low DIC values in both regions, and slight increase in TA (9.1 \pm 29.2 μ mol kg⁻¹ from March 2022 to May 2022; Fig. 4b), above the

mixing line (Fig. 3b). The relationship in Figure 6 also indicates that primary production is influenced by nitrate and silicate availability. Nitrate concentrations decreased substantially from 65 μmol kg⁻¹ in March to 22 μmol kg⁻¹ in May 2022 (Fig. 6; Fig. S4), coinciding with the period of intense primary production. This significant drawdown in nitrate concentrations suggests that nitrate assimilation was the primary driver of the observed decrease in DIC and the slight increase in TA during this period. Nitrate assimilation involves the consumption of hydrogen ions (H⁺) and the release of hydroxide ions (OH⁻), which leads to an increase in pH and, consequently, in TA (Brenner et al., 2016; Wolf-Gladrow et al., 2007). Therefore, nitrate assimilation played a crucial role in shaping the carbonate system dynamics by decreasing CO₂ and DIC, while increasing TA. The regression analysis of ΔNO₃⁻ and ΔDIC between March and May 2022 revealed a slope of 6.90 for the changes in nitrate concentrations (Fig. 6), which is close to the Redfield ratio of 6.625 for the C:N ratio (Redfield et al., 1963). This close match suggests nitrate assimilation during the spring bloom, which is closely linked to a reduction in DIC. Similarly, the ΔSiO₂ regression produced a slope of 8.11 (Fig. 6), which is also close to the Redfield ratio for SiO₂ (7.067), further supporting the conclusion that the enhanced primary production in this region during the spring bloom contributed to nutrient uptake, particularly nitrate and silicate.

We therefore propose that assimilation of NO_3^- during the time of intense primary production in May 2022 could explain the local increase of total alkalinity during the spring bloom. First, the maximum concentration of NO_3^- was captured in March before the high biologically productive season started in May 2022 (Fig. 4 - 7), with maximum concentrations measured in the Western WS. A significant drawdown of NO_3^- from the maximum value of 65 μ mol kg⁻¹ in March 2022 to 22 μ mol kg⁻¹ in May 2022, resulted in an average decrease of $19.2 \pm 9.6 \mu$ mol kg⁻¹ of NO_3^- (Fig. 6; Fig. S4). Brewer and Goldman (1976) also documented that nitrate assimilation increases TA ($9.1 \pm 29.2 \mu$ mol kg⁻¹).

An uptake of NH₄⁺ was not obvious, because NH₄⁺ concentrations were much lower during this period (Fig. S4), suggesting only a small impact on TA patterns. Therefore, the limited influence of NH₄⁺ uptake further emphasizes the central role of nitrate assimilation in shaping the observed patterns in the carbonate system. Nitrification, the process by which NH₄⁺ is converted into NO₂⁻, causes a decrease in TA by 2 moles per mole of nitrogen (Wolf-Gladrow et al., 2007; Xue and Cai, 2020), thus has the opposite effect compared to nitrate assimilation, which increases TA. The decrease in NO₃⁻ from May to July 2022 was less pronounced (1.51 \pm 5.16 μ mol kg⁻¹, Fig. 6), which is consistent with the general trend of lower NO₃⁻ concentrations in summer, likely driven by higher turnover rates (Kieskamp et al., 1991).

5 Conclusion

The findings highlight significant regional and seasonal variations in the EFWS carbonate system, reflecting broader carbon dynamics in coastal and shelf seas. Both TA and DIC exhibit substantial variations across regions and seasons, with a notable decrease in DIC from East to West and an increase in TA during biologically productive periods, such as spring and summer. In spring 2022, a significant drawdown of NO₃⁻ was observed, correlating with a slight increase in TA, likely due to nitrate assimilation during primary production. Primary production could explain up to 88 % of the ΔDIC_{excess} in the Western WS and

up to 92 % in the Eastern WS, contributing to the significant drop in DIC, slight TA production, and NO₃⁻ drawdown during this period.

In the summer, it is likely that the remineralization of organic matter, combined with the dissolution of CaCO₃ in sediments, contributes to higher TA production, especially in the coastal and nearshore areas of the Western EFWS. On the other hand, the Eastern EFWS may experience greater CaCO₃ formation, which may reduce TA levels ([TA-DIC] < 200 μmol kg⁻¹). However, the region still acts as a net source of TA, in part due to the known high rates of benthic anaerobic respiration, such as organic matter decomposition and associated TA production, particularly after the high productivity of the spring season. This TA generation may enhance the region's capacity to absorb CO₂, despite the broader southern North Sea generally being considered a carbon source to the atmosphere. These findings emphasize the complexity of the biogeochemical processes driving regional and seasonal variability in the EFWS carbonate system, particularly those influenced by tidal cycles, river inputs, and sediment interactions. Riverine inputs, especially from the Ems River estuary, also influence local carbonate chemistry. However, the relatively low river inflows during the summer suggest that sediment processes, such as organic matter decomposition, may play a more dominant role.

To gain a comprehensive understanding of these intricate interactions and their impact on carbon storage and marine biogeochemistry in this ecologically important region, further research, including sediment studies and continuous tidal monitoring, is essential. This study is the first to combine the analysis of [TA-DIC] with other parameters such as ΔTA_{excess}, ΔDIC_{excess}, and ΔTA_P to infer underlying biogeochemical processes - such as biological productivity and nutrient availability. This innovative approach offers a new way to examine how various environmental factors interact and influence the carbonate system. The results have the potential to refine existing models of the biogeochemical cycle, providing valuable insights for more accurate climate predictions and improved strategies for managing coastal systems in response to environmental change.

Code and data availability

460

465

470

475

480

485

The data supporting our findings in this study have been submitted by Lara Luitjens (NLWKN) to the PANGAEA data repository and are currently undergoing final editorial processing. A DOI for the dataset will be available upon completion of the review process (Luitjens et al., in review). The datasets can be accessed through the following links:

https://doi.pangaea.de/10.1594/PANGAEA.974424

https://doi.pangaea.de/10.1594/PANGAEA.974426

https://doi.pangaea.de/10.1594/PANGAEA.974427

https://doi.pangaea.de/10.1594/PANGAEA.974428

Competing interests

The contact author has declared that none of the authors has any competing interests.

Acknowledgements

490

495

We thank Martina Gehrung, Tanja Pieplow and Catharina Petrauskas for their exceptional technical support, meticulous work and dedication. They ensured the reliability and accuracy of our data through their careful handling of samples and precise analytical measurements. The scientists and crew who participated in the research expeditions, including the captain Alexander Heidenreich and the crew of the *RV Burchana* (Jens Voß and Winfried Bruns) are also greatly appreciated. It was their hard work, professionalism and co-operation during the challenging field work that made it possible to collect the data required for this study. The success of our research would not have been possible without your tireless efforts at sea. We thank all of you for your unwavering support and commitment.

Finally, we would like to acknowledge the support and valuable discussions with the members of the "CARBOSTORE" project and especially Prof. Dr. habil. Michael Böttcher from the Institute for Baltic Sea Research in Warnemünde (Germany).

The author wishes to express their gratitude to the anonymous reviewer for their constructive comments and valuable feedback, which significantly enhanced the manuscript.

Financial support

This research was funded through the "CARBOSTORE" project (Grant Number 03F0875A), by the German Federal Ministry of Education and Research (BMBF). Additionally, the Helmholtz-Zentrum Hereon covered the article processing charges for this open-access publication.

References

- 4H Jena engineering GmbH: Data Processing for CONTROS HydroC ® CO2 (Manual), 1–7 pp., 2021.
- Al-Raei, A. M., Bosselmann, K., Böttcher, M. E., Hespenheide, B., and Tauber, F.: Seasonal dynamics of microbial sulfate reduction in temperate intertidal surface sediments: controls by temperature and organic matter, Ocean Dyn, 59, 351–370, https://doi.org/10.1007/s10236-009-0186-5, 2009.
 - Artioli, Y., Blackford, J. C., Butenschön, M., Holt, J. T., Wakelin, S. L., Thomas, H., Borges, A. V., and Allen, J. I.: The carbonate system in the North Sea: Sensitivity and model validation, Journal of Marine Systems, 102–104, 1–13, https://doi.org/10.1016/j.jmarsys.2012.04.006, 2012.
- Bauer, J. E., Cai, W. J., Raymond, P. A., Bianchi, T. S., Hopkinson, C. S., and Regnier, P. A. G.: The changing carbon cycle of the coastal ocean, https://doi.org/10.1038/nature12857, 2013.
 - Beck, M. and Brumsack, H. J.: Biogeochemical cycles in sediment and water column of the Wadden Sea: The example Spiekeroog Island in a regional context, Ocean Coast Manag, 68, 102–113, https://doi.org/10.1016/j.ocecoaman.2012.05.026, 2012.

- Van Beusekom, J. E. E. and De Jonge, V. N.: Long-term changes in Wadden Sea nutrient cycles: Importance of organic matter import from the North Sea, Hydrobiologia, 475–476, 185–194, https://doi.org/10.1023/A:1020361124656, 2002.
 - Van Beusekom, J. E. E., Brockmann, U. H., Hesse, K.-J., Hickel, W., Poremba, K., and Tillmann, U.: The importance of sediments in the transformation and turnover of nutrients and organic matter in the Wadden Sea and German Bight, Deutsche Hydrographische Zeitschrift, 51, 245–266, https://doi.org/10.1007/BF02764176, 1999.
- Van Beusekom, J. E. E., Buschbaum, C., and Reise, K.: Wadden Sea tidal basins and the mediating role of the North Sea in ecological processes: scaling up of management?, Ocean Coast Manag, 68, 69–78, https://doi.org/10.1016/j.ocecoaman.2012.05.002, 2012.
 - Borges, A. V., Schiettecatte, L.-S., Abril, G., Delille, B., and Gazeau, F.: Carbon dioxide in European coastal waters, Estuar Coast Shelf Sci, 70, 375–387, https://doi.org/10.1016/j.ecss.2006.05.046, 2006.
- Borges, A. V., Speeckaert, G., Champenois, W., Scranton, M. I., and Gypens, N.: Productivity and Temperature as Drivers of Seasonal and Spatial Variations of Dissolved Methane in the Southern Bight of the North Sea, Ecosystems, 21, 583–599, https://doi.org/10.1007/s10021-017-0171-7, 2017.
- Böttcher, M. E., Oelschläger, B., Höpner, T., Brumsack, H. J., and Rullkötter, J.: Sulfate reduction related to the early diagenetic degradation of organic matter and "black spot" formation in tidal sandflats of the German Wadden Sea (southern North Sea): Stable isotope (¹³C, ³⁴S, ¹⁸O) and other geochemical results, Org Geochem, 29, 1517–1530, https://doi.org/10.1016/S0146-6380(98)00124-7, 1998.
 - Brasse, S., Reimer, A., Seifert, R., and Michaelis, W.: The influence of intertidal mudflats on the dissolved inorganic carbon and total alkalinity distribution in the German Bight, southeastern North Sea, Journal of Sea Research, 93–103 pp., 1999.
 - Brenner, H., Braeckman, U., Le Guitton, M., and Meysman, F. J. R.: The impact of sedimentary alkalinity release on the water column CO₂ system in the North Sea, Biogeosciences, 13, 841–863, https://doi.org/10.5194/bg-13-841-2016, 2016.

- Brewer, P. G. and Goldman, J. C.: Alkalinity changes generated by phytoplankton growth, Limnol Oceanogr, 21, 108–117, https://doi.org/10.4319/lo.1976.21.1.0108, 1976.
- Burt, W. J., Thomas, H., Hagens, M., Pätsch, J., Clargo, N. M., Salt, L. A., Winde, V., and Böttcher, M. E.: Carbon sources in the North Sea evaluated by means of radium and stable carbon isotope tracers, Limnol Oceanogr, 61, 666–683, https://doi.org/10.1002/lno.10243, 2016.
- Chen, C. A. and Wang, S.: Carbon, alkalinity and nutrient budgets on the East China Sea continental shelf, J Geophys Res Oceans, 104, 20675–20686, https://doi.org/10.1029/1999JC900055, 1999.
- Chen, C.-T. A.: Decomposition of Calcium Carbonate and Organic Carbon in the Deep Oceans, Science (1979), 201, 735–736, https://doi.org/10.1126/science.201.4357.735, 1978.
- Dickson, A. G.: An exact definition of total alkalinity and a procedure for the estimation of alkalinity and total inorganic carbon from titration data, Deep Sea Research Part A. Oceanographic Research Papers, 28, 609–623, https://doi.org/10.1016/0198-0149(81)90121-7, 1981.

- Duan, L., Song, J., Li, X., Yuan, H., and Zhuang, W.: Potential risks of CO₂ removal project based on carbonate pump to marine ecosystem, https://doi.org/10.1016/j.scitotenv.2022.160728, 1 March 2023.
- Feely, R., Doney, S., and Cooley, S.: Ocean Acidification: Present Conditions and Future Changes in a High-CO₂ World, Oceanography, 22, 36–47, https://doi.org/10.5670/oceanog.2009.95, 2009.
 - Friedlingstein, P., O'Sullivan, M., Jones, M. W., Andrew, R. M., Bakker, D. C. E., Hauck, J., Landschützer, P., Le Quéré, C., Luijkx, I. T., Peters, G. P., Peters, W., Pongratz, J., Schwingshackl, C., Sitch, S., Canadell, J. G., Ciais, P., Jackson, R. B., Alin, S. R., Anthoni, P., Barbero, L., Bates, N. R., Becker, M., Bellouin, N., Decharme, B., Bopp, L., Brasika, I. B. M.,
- Cadule, P., Chamberlain, M. A., Chandra, N., Chau, T.-T.-T., Chevallier, F., Chini, L. P., Cronin, M., Dou, X., Enyo, K., Evans, W., Falk, S., Feely, R. A., Feng, L., Ford, D. J., Gasser, T., Ghattas, J., Gkritzalis, T., Grassi, G., Gregor, L., Gruber, N., Gürses, Ö., Harris, I., Hefner, M., Heinke, J., Houghton, R. A., Hurtt, G. C., Iida, Y., Ilyina, T., Jacobson, A. R., Jain, A., Jarníková, T., Jersild, A., Jiang, F., Jin, Z., Joos, F., Kato, E., Keeling, R. F., Kennedy, D., Klein Goldewijk, K., Knauer, J., Korsbakken, J. I., Körtzinger, A., Lan, X., Lefèvre, N., Li, H., Liu, J., Liu, Z., Ma, L., Marland, G., Mayot, N., McGuire.
- P. C., McKinley, G. A., Meyer, G., Morgan, E. J., Munro, D. R., Nakaoka, S.-I., Niwa, Y., O'Brien, K. M., Olsen, A., Omar, A. M., Ono, T., Paulsen, M., Pierrot, D., Pocock, K., Poulter, B., Powis, C. M., Rehder, G., Resplandy, L., Robertson, E., Rödenbeck, C., Rosan, T. M., Schwinger, J., Séférian, R., et al.: Global Carbon Budget 2023, Earth Syst Sci Data, 15, 5301–5369, https://doi.org/10.5194/essd-15-5301-2023, 2023.
- Gao, H., Schreiber, F., Collins, G., Jensen, M. M., Kostka, J. E., Lavik, G., De Beer, D., Zhou, H. Y., and Kuypers, M. M. M.:
 Aerobic denitrification in permeable Wadden Sea sediments, ISME Journal, 4, 417–426, https://doi.org/10.1038/ismej.2009.127, 2010.
 - Gattuso, J. P., Frankignoulle, M., and Wollast, R.: Carbon and carbonate metabolism in coastal aquatic ecosystems, Annu Rev Ecol Syst, 29, 405–434, https://doi.org/10.1146/annurev.ecolsys.29.1.405, 1998.
- Gruber, N., Clement, D., Carter, B. R., Feely, R. A., van Heuven, S., Hoppema, M., Ishii, M., Key, R. M., Kozyr, A., Lauvset,
 S. K., Lo Monaco, C., Mathis, J. T., Murata, A., Olsen, A., Perez, F. F., Sabine, C. L., Tanhua, T., and Wanninkhof, R.:
 The oceanic sink for anthropogenic CO₂ from 1994 to 2007, Science (1979), 363, 1193–1199, https://doi.org/10.1126/science.aau5153, 2019.
 - Grunwald, M., Dellwig, O., Beck, M., Dippner, J. W., Freund, J. A., Kohlmeier, C., Schnetger, B., and Brumsack, H. J.: Methane in the southern North Sea: Sources, spatial distribution and budgets, Estuar Coast Shelf Sci, 81, 445–456, https://doi.org/10.1016/j.ecss.2008.11.021, 2009.

- Herrling, G. and Winter, C.: Tidally- and wind-driven residual circulation at the multiple-inlet system East Frisian Wadden Sea, Cont Shelf Res, 106, 45–59, https://doi.org/10.1016/j.csr.2015.06.001, 2015.
- Hoppema, J. M. J.: The distribution and seasonal variation of alkalinity in the Southern Bight of the North Sea and in the Western Wadden Sea, Netherlands Journal of Sea Research, 26, 11–23, https://doi.org/10.1016/0077-7579(90)90053-J, 1990.

- Hu, X. and Cai, W. J.: An assessment of ocean margin anaerobic processes on oceanic alkalinity budget, Global Biogeochem Cycles, 25, https://doi.org/10.1029/2010GB003859, 2011.
- Jiang, L. Q., Cai, W. J., and Wang, Y.: A comparative study of carbon dioxide degassing in river- and marine-dominated estuaries, Limnol Oceanogr, 53, 2603–2615, https://doi.org/10.4319/lo.2008.53.6.2603, 2008.
- Joesoef, A., Huang, W. J., Gao, Y., and Cai, W. J.: Air-water fluxes and sources of carbon dioxide in the Delaware Estuary: Spatial and seasonal variability, Biogeosciences, 12, 6085–6101, https://doi.org/10.5194/bg-12-6085-2015, 2015.
 - Kamyshny, A. and Ferdelman, T. G.: Dynamics of zero-valent sulfur species including polysulfides at seep sites on intertidal sand flats (Wadden Sea, North Sea), Mar Chem, 121, 17–26, https://doi.org/10.1016/j.marchem.2010.03.001, 2010.
- Kieskamp, W., Lohse, L., Epping, E., and Helder, W.: Seasonal variation in denitrification rates and nitrous oxide fluxes in intertidal sediments of the western Wadden Sea, Mar Ecol Prog Ser, 72, 145–151, https://doi.org/10.3354/meps072145, 1991.
 - Kowalski, N., Dellwig, O., Beck, M., Gräwe, U., Neubert, N., Nägler, T. F., Badewien, T. H., Brumsack, H.-J., van Beusekom, J. E. E., and Böttcher, M. E.: Pelagic molybdenum concentration anomalies and the impact of sediment resuspension on the molybdenum budget in two tidal systems of the North Sea, Geochim Cosmochim Acta, 119, 198–211, https://doi.org/10.1016/j.gca.2013.05.046, 2013.

- Kroeker, K. J., Kordas, R. L., Crim, R., Hendriks, I. E., Ramajo, L., Singh, G. S., Duarte, C. M., and Gattuso, J. P.: Impacts of ocean acidification on marine organisms: Quantifying sensitivities and interaction with warming, Glob Chang Biol, 19, 1884–1896, https://doi.org/10.1111/gcb.12179, 2013.
- Legge, O., Johnson, M., Hicks, N., Jickells, T., Diesing, M., Aldridge, J., Andrews, J., Artioli, Y., Bakker, D. C. E., Burrows,
 M. T., Carr, N., Cripps, G., Felgate, S. L., Fernand, L., Greenwood, N., Hartman, S., Kröger, S., Lessin, G., Mahaffey, C.,
 Mayor, D. J., Parker, R., Queirós, A. M., Shutler, J. D., Silva, T., Stahl, H., Tinker, J., Underwood, G. J. C., Van Der Molen, J., Wakelin, S., Weston, K., and Williamson, P.: Carbon on the Northwest European Shelf: Contemporary Budget and Future Influences, Front Mar Sci, 7, https://doi.org/10.3389/fmars.2020.00143, 2020.
- Lehmann, N., Stacke, T., Lehmann, S., Lantuit, H., Gosse, J., Mears, C., Hartmann, J., and Thomas, H.: Alkalinity responses to climate warming destabilise the Earth's thermostat, Nat Commun, 14, https://doi.org/10.1038/s41467-023-37165-w, 2023.
 - Li, X., Wu, Z., Ouyang, Z., and Cai, W.-J.: The source and accumulation of anthropogenic carbon in the U.S. East Coast, Sci Adv, 10, 3169, https://doi.org/10.1126/sciadv.adl3169, 2024.
- Liang, H., Lunstrum, A. M., Dong, S., Berelson, W. M., and John, S. G.: Constraining CaCO₃ Export and Dissolution With an Ocean Alkalinity Inverse Model, Global Biogeochem Cycles, 37, https://doi.org/10.1029/2022GB007535, 2023.
 - Lorkowski, I., Pätsch, J., Moll, A., and Kühn, W.: Interannual variability of carbon fluxes in the North Sea from 1970 to 2006 Competing effects of abiotic and biotic drivers on the gas-exchange of CO₂, Estuar Coast Shelf Sci, 100, 38–57, https://doi.org/10.1016/j.ecss.2011.11.037, 2012.

- Luitjens, L.: Analytische Messung auserwählter Nährstoffkonzentrationen im ökologischen System Wattenmeer und Ems, sowie deren Entwicklung, Einflüsse und Auswirkungen, Unpublished master`s thesis, 2019.
 - Macovei, V. A., Petersen, W., Brix, H., and Voynova, Y. G.: Reduced Ocean Carbon Sink in the South and Central North Sea (2014–2018) Revealed From FerryBox Observations, Geophys Res Lett, 48, 1–11, https://doi.org/10.1029/2021GL092645, 2021.
- Norbisrath, M., Van Beusekom, J. E. E., and Thomas, H.: Alkalinity sources in the Dutch Wadden Sea, Ocean Science, 20, 1423–1440, https://doi.org/10.5194/os-20-1423-2024, 2024.
 - Orr, J. C., Fabry, V. J., Aumont, O., Bopp, L., Doney, S. C., Feely, R. A., Gnanadesikan, A., Gruber, N., Ishida, A., Joos, F., Key, R. M., Lindsay, K., Maier-Reimer, E., Matear, R., Monfray, P., Mouchet, A., Najjar, R. G., Plattner, G. K., Rodgers, K. B., Sabine, C. L., Sarmiento, J. L., Schlitzer, R., Slater, R. D., Totterdell, I. J., Weirig, M. F., Yamanaka, Y., and Yool, A.: Anthropogenic ocean acidification over the twenty-first century and its impact on calcifying organisms, Nature, 437, 681–686, https://doi.org/10.1038/nature04095, 2005.
 - Pätsch, J. and Lenhart, H.: Daily Loads of Nutrients, Total Alkalinity, Dissolved Inorganic Carbon and Dissolved Organic Carbon of the European Continental Rivers for the Years 1977-2002, 48–159 pp., Berichte aus dem Zentrum für Meeresund Klimaforschung, Reihe B, Ozeanographie, 2004.
- Postma, H.: Exchange of materials between the North Sea and the Wadden Sea, Mar Geol, 40, 199–213, https://doi.org/10.1016/0025-3227(81)90050-5, 1981.

- Prowe, A. E. F., Thomas, H., Pätsch, J., Kühn, W., Bozec, Y., Schiettecatte, L. S., Borges, A. V., and de Baar, H. J. W.: Mechanisms controlling the air-sea CO₂ flux in the North Sea, Cont Shelf Res, 29, 1801–1808, https://doi.org/10.1016/j.csr.2009.06.003, 2009.
- Redfield, A. C., Ketchum, B. H., and Richards, F. A.: The influence of organisms on the composition of seawater, The sea, 2, 635 26–77, 1963.
 - Ricour, F., Guidi, L., Gehlen, M., DeVries, T., and Legendre, L.: Century-scale carbon sequestration flux throughout the ocean by the biological pump, Nat Geosci, 16, 1105–1113, https://doi.org/10.1038/s41561-023-01318-9, 2023.
 - Sabine, C. L., Feely, R. A., Gruber, N., Key, R. M., Lee, K., Bullister, J. L., Wanninkhof, R., Wong, C. S., Wallace, D. W. R., Tilbrook, B., Millero, F. J., Peng, T.-H., Kozyr, A., Ono, T., and Rios, A. F.: The Oceanic Sink for Anthropogenic CO₂, Science (1979), 305, 367–371, https://doi.org/10.1126/science.1097403, 2004.
 - Santos, I. R., Beck, M., Brumsack, H. J., Maher, D. T., Dittmar, T., Waska, H., and Schnetger, B.: Porewater exchange as a driver of carbon dynamics across a terrestrial-marine transect: Insights from coupled ²²²Rn and pCO₂ observations in the German Wadden Sea, Mar Chem, 171, 10–20, https://doi.org/10.1016/j.marchem.2015.02.005, 2015.
- Schwichtenberg, F.: Drivers of the carbonate system variability in the southern North Sea: River input, anaerobic alkalinity generation in the Wadden Sea and internal processes, 2013.
 - Schwichtenberg, F., Pätsch, J., Ernst Böttcher, M., Thomas, H., and Winde, V.: The impact of intertidal areas on the carbonate system of the southern North Sea, Biogeosciences, 17, 4223–4245, https://doi.org/10.5194/bg-17-4223-2020, 2020.

- Staneva, J., Stanev, E. V., Wolff, J. O., Badewien, T. H., Reuter, R., Flemming, B., Bartholomä, A., and Bolding, K.: Hydroynamics and sediment dynamics in the German Bight. A focus on observations and numerical modelling in the East Frisian Wadden Sea, Cont Shelf Res, 29, 302–319, https://doi.org/10.1016/j.csr.2008.01.006, 2009.
 - Thomas, H., Bozec, Y., Elkalay, K., de Baar, H. J. W., Borges, A. V., and Schiettecatte, L.-S.: Controls of the surface water partial pressure of CO₂ in the North Sea, Biogeosciences, 2, 323–334, https://doi.org/10.5194/bg-2-323-2005, 2005.
 - Thomas, H., Prowe, A. E. F., van Heuven, S., Bozec, Y., de Baar, H. J. W., Schiettecatte, L. S., Suykens, K., Koné, M., Borges, A. V., Lima, I. D., and Doney, S. C.: Rapid decline of the CO₂ buffering capacity in the North Sea and implications for the North Atlantic Ocean, Global Biogeochem Cycles, 21, https://doi.org/10.1029/2006GB002825, 2007.
 - Thomas, H., Schiettecatte, L.-S., Suykens, K., Koné, Y. J. M., Shadwick, E. H., Prowe, A. E. F., Bozec, Y., de Baar, H. J. W., and Borges, A. V.: Enhanced ocean carbon storage from anaerobic alkalinity generation in coastal sediments, Biogeosciences, 6, 267–274, https://doi.org/10.5194/bg-6-267-2009, 2009.
 - UNESCO World Heritage Centre: https://whc.unesco.org/en/list/1314/, last access: 23 March 2025, n.d.

- Voynova, Y. G., Petersen, W., Gehrung, M., Aßmann, S., and King, A. L.: Intertidal regions changing coastal alkalinity: The Wadden Sea-North Sea tidally coupled bioreactor, Limnol Oceanogr, 64, 1135–1149, https://doi.org/10.1002/lno.11103, 2019.
 - Wolf-Gladrow, D. A., Zeebe, R. E., Klaas, C., Körtzinger, A., and Dickson, A. G.: Total alkalinity: The explicit conservative expression and its application to biogeochemical processes, Mar Chem, 106, 287–300, https://doi.org/10.1016/j.marchem.2007.01.006, 2007.
 - Wu, C. S., Røy, H., and de Beer, D.: Methanogenesis in sediments of an intertidal sand flat in the Wadden Sea, Estuar Coast Shelf Sci, 164, 39–45, https://doi.org/10.1016/j.ecss.2015.06.031, 2015.
 - Xue, L. and Cai, W. J.: Total alkalinity minus dissolved inorganic carbon as a proxy for deciphering ocean acidification mechanisms, Mar Chem, 222, https://doi.org/10.1016/j.marchem.2020.103791, 2020.
- Kue, L., Cai, W. J., Sutton, A. J., and Sabine, C.: Sea surface aragonite saturation state variations and control mechanisms at the Gray's Reef time-series site off Georgia, USA (2006–2007), Mar Chem, 195, 27–40, https://doi.org/10.1016/j.marchem.2017.05.009, 2017.